1 Adsorption Kinetics for CO<sub>2</sub> Capture using Cerium Oxide Impregnated on Activated

2 carbon

3

4 Azizul Hakim Lahuri<sup>1\*</sup>, Michael Ling Nguang Khai<sup>2</sup>, Afidah Abdul Rahim<sup>2</sup>, Norazzizi Nordin<sup>2</sup>

5

- 6 <sup>1</sup>Department of Science and Technology, Faculty of Agriculture, Science and Technology,
- 7 Universiti Putra Malaysia Bintulu Campus, P.O Box 396, Nyabau Road, 97008 Bintulu,
- 8 Sarawak, Malaysia.

9

- <sup>2</sup>School of Chemical Sciences, Universiti Sains Malaysia, 11800 Gelugor, Pulau Pinang,
- 11 Malaysia.

12

\*Corresponding author: azizulhakim@upm.edu.my

14

#### 15 ABSTRACT

- Various metal oxides of CeO<sub>2</sub>, ZnO, and Co<sub>3</sub>O<sub>4</sub> impregnated on AC were synthesized to
- determine the CO<sub>2</sub> capture efficiency and analyze with adsorption kinetics model. Batch kinetic
- studies showed that CeO<sub>2</sub>/AC is the most efficient adsorbent with an equilibrium time of 10
- minutes was needed to obtain adsorption capacity of 52.68 mg/g. CO<sub>2</sub> adsorption at 30 °C
- 20 exhibits the optimum temperature with only 6.53% loss in adsorption capacity after 5 cycles of
- 21 CO<sub>2</sub> adsorption-desorption. The CeO<sub>2</sub> on AC was detected through XRD and the SEM image
- shows well-distributed CeO<sub>2</sub> particles on AC surfaces. CO<sub>2</sub> adsorption at 30 °C shows best
- 23 fitted with pseudo-second-order kinetics with the R<sup>2</sup> is 0.9994 and the relative error between
- calculated and experimental adsorption capacity is only 1.32%. The adsorption considering
- 25 chemisorption responsible for improving adsorption capacity. The addition of CeO<sub>2</sub> on AC
- 26 enhanced the adsorption capacity by providing active sites to attract CO<sub>2</sub>.

27 28

29 **Keywords:** CO<sub>2</sub> capture; adsorption kinetics; cerium (IV) oxide; activated carbon; recyclability

30 31

#### 1. **INTRODUCTION**

- Human population evolution leads to an increase in energy consumption as well as CO<sub>2</sub> gas
- production from transportation and developing industrial activities. CO<sub>2</sub> is one of the major
- 34 greenhouse gases that has eventually induced growing concern among the communities due to

its environmental effects. Based on National Oceanic and Atmospheric Administration (NOAA)<sup>1</sup>, the global CO<sub>2</sub> concentration in the earth's atmosphere during January 2020 was reported to be 413.40 ppm or which accounts for an increment of 0.63 % compared to 410.83 ppm in January 2019. The current annual mean global CO<sub>2</sub> growth rate at approximately 2.94 ppm in 2019 may cause severe climatic change such as global warming and a rise in seawater level<sup>2</sup>.

The large emission of CO<sub>2</sub> gas from fossil fuel power plants led to a Carbon Capture and Storage (CCS) process which aims to reduce CO<sub>2</sub> emission from a large point source<sup>3</sup>. In September 2008, an integrated pilot-scale CCS power plant has started operating and estimated to account for a reduction in CO<sub>2</sub> emission up to approximately 80 % compared to power plants without CCS<sup>4</sup>. In order to sustain a better environment for future generations, several approaches to sorption-based technologies were developed to reduce environmental pollution caused by the mass emission of CO<sub>2</sub> gas.

Adsorption technologies as an alternative to the most mature amine-based solvent processes<sup>5</sup> have started to be considered in the early 1990's<sup>6</sup>. Liquid amine-based absorbent suffers from a series of unfavorable conditions including the corrosive nature of amines, high cost and high regeneration energy<sup>7</sup>. Therefore solid adsorbents which has a wider temperature range of regeneration, yielding less waste during recycling and with an easier disposing of the procedure of spent adsorbent<sup>8</sup>. Among these technologies, adsorption-based is preferred over absorption-based due to the drawbacks of absorption with aqueous alkanolamine solutions such as high equipment corrosion rate, high energy consumption in regeneration and a large absorbent volume required while adsorbents such as amine-based chemical adsorbents with large surface area, large CO<sub>2</sub> adsorption capacity, high adsorption and desorption rates, high tolerance to moisture, and high selectivity towards CO<sub>2</sub><sup>9</sup>. Furthermore, Yu *et al.* also reported that 60 % of total energy is consumed for the regeneration of CO<sub>2</sub>-rich chemical absorbents<sup>9</sup>.

CO<sub>2</sub> adsorption on solid sorbents can be classified into two mechanisms namely physical adsorption which involving intermolecular forces and chemical adsorption which involve the sharing of electrons by the adsorbent and the adsorbate<sup>10</sup>. The emergence of active researches toward solid CO<sub>2</sub> adsorbents along with their properties and performances provides good insights into further developing the progress in this field. Among the adsorption-based sorbents, it includes the low-temperature solid adsorbents (< 200 °C) such as carbon-based adsorbents<sup>11</sup>,

zeolite-based adsorbents<sup>12</sup>, metal-organic framework based adsorbents<sup>13</sup>, alkali metal carbonate-based adsorbents<sup>14</sup>, amine-based solid adsorbents<sup>15</sup>, the intermediate-temperature solid adsorbents (200-400 °C) and high-temperature solid adsorbents (> 400 °C) such as calcium-based adsorbents<sup>16</sup> and alkali ceramic-based adsorbents<sup>7</sup>. Hence, a further modification to obtain easy handling than liquid absorbent by using support materials to impregnate the amine-based sorbent. Several amine-based adsorbents were reported monoethanolamine (MEA) on AC<sup>17</sup> exhibits low adsorption capacity (15.40 mg/g) due to the large molecule coating the AC microporous surfaces. Kamarudin et al. 18 have reported various types of amine-functionalized kenaf with tetraethylenepentamine (TEPA) on kenaf showed the highest adsorption capacity (40.22 mg/g) than MEA on kenaf and raw kenaf. A larger molecule of octadecylamine (ODA) on silica gel (SG) which pre-treated at 600 °C was found similarly adsorption capacity (15.61 mg/g)<sup>15</sup> with MEA on AC.

The calcium-based adsorbent is a classically used metal oxide adsorbent for capturing CO<sub>2</sub> due to its high reactivity with CO<sub>2</sub> and low-cost material. The reversible reaction between CaO and CO<sub>2</sub> is shown in Equation 1. The forward reaction depicts the adsorption of CO<sub>2</sub> at a temperature between 600 to 700 °C<sup>7</sup> to form CaCO<sub>3</sub> while backward reaction depicts the regeneration of CO<sub>2</sub> but requires high heat supply up to 900 to 950 °C for next cycle of CO<sub>2</sub> adsorption<sup>19-21</sup>.

89 
$$\operatorname{CaO}(s) + \operatorname{CO}_2(g) \rightleftharpoons \operatorname{CaCO}_3$$
 (1)

Therefore, an alternative metal oxide was used as adsorbent of CO<sub>2</sub> such as iron oxides (FeO, Fe<sub>2</sub>O<sub>3</sub>, and Fe<sub>3</sub>O<sub>4</sub>)<sup>22</sup>, TiO<sub>2</sub><sup>23</sup>, γ-Al<sub>2</sub>O<sub>3</sub><sup>23</sup>, CeO<sub>2</sub><sup>24</sup>, SiO<sub>2</sub><sup>24</sup>, ZrO<sub>2</sub><sup>24</sup>, and ZnO<sub>2</sub><sup>25</sup>. According to Chanapattharapol *et al.*<sup>10</sup>, iron oxide doped MCM-41 adsorbent prepared by impregnation reported higher CO<sub>2</sub> adsorption than the undoped MCM-41 partly due to increased surface area and electron transfer from metal to CO<sub>2</sub>. Numerous studies were reported on CO<sub>2</sub> adsorption on activated carbon (AC) due to it is widely available, low cost, and green product. However, AC only offers a weak interaction by physisorption<sup>22</sup>. Thus, surface modification on the carbonaceous support can contribute to higher selectivity towards CO<sub>2</sub> and increase the adsorption capacity of the porous material. AC surface modification by adding metal oxide of alkali metal, alkaline earth metal, and transition metal provides basicity sites on the AC surfaces. A study reported a successful surface modification of AC loaded with Fe<sub>2</sub>O<sub>3</sub> with 103.7 mg/g adsorbent with physisorption mainly contributed by AC and chemisorption

contributed by Fe<sub>2</sub>O<sub>3</sub><sup>26</sup>. Other studies were reported using NiO<sup>27</sup>, MgO<sup>28</sup> and CuO<sup>29</sup> to modify the AC surfaces and enhance its adsorption capacity. It is notably metal oxide loading on AC increase the adsorption capacity due to significantly attract more CO<sub>2</sub> to be chemically bonded and provide better chemisorption properties for the adsorbent.

Recently, ionic liquid-based and deep eutectic solvent (DES)-based materials were applied to the CO<sub>2</sub> capture. Marliza et al. reported ionic liquid functionalized SiO<sub>2</sub> shows highest 1-butyl-3-methylimidazolium adsorption capacity for trifluoromethanesulfonate, [bmim][CF<sub>3</sub>SO<sub>3</sub>]/SiO<sub>2</sub> than SiO<sub>2</sub> only<sup>32</sup>. Addition of NiO to the 1-ethyl-3-methylimidazolium hydrogensulfate, [emim][HSO<sub>4</sub>] functionalized SiO<sub>2</sub> shows enhance in adsorption capacity due to higher surface area than 10%[emim][HSO<sub>4</sub>]/SiO<sub>2</sub><sup>33</sup>. Green technology application through the DES of Choline chloride: urea (ChCl:U) is biocompatible, non-toxic, biodegradable, inexpensive and easy to prepare<sup>34</sup>. The ChCl:U functionalized silica gel was found to have lower adsorption capacity (22.30 mg/g) due to lower surface area (317.50 m<sup>2</sup>/g)<sup>34</sup> of the adsorbent rather than ChCl:U functionalized AC<sup>35</sup> which exhibits higher surface area (581.23 m<sup>2</sup>/g) and adsorption capacity. Nonetheless, the significance of desorption properties for the adsorbents are not reported for these works. The performance of various adsorbents was tabulated in Table 1.

In the present work, double activation will be performed on AC to reactivate the surfaces. The metal oxides of ZnO, CeO<sub>2</sub>, and Co<sub>3</sub>O<sub>4</sub> was added to the modified AC. These metal oxides were chosen based on the previous study which the metal oxides on AC are not yet discovered its adsorption capacity and adsorption kinetics. Hence, the specific aim of this work is to measure the adsorption capacity, evaluate the desorption properties, identify the most efficient metal loaded on AC, and determine optimum adsorption temperature with adsorption kinetics analysis for  $CO_2$  capture.

**Table 1.** Adsorption capacities of various adsorbents.

Adsorbent	Adsorption	Adsorption	CO <sub>2</sub>	Sources
	Capacity	Temperature	Purity	
	(mg/g)	(°C)		
35%ODA/SG600	15.61	25	99 %	15
MEA/AC	15.40	25	15 %	16
Raw kenaf	27.46	30	99.99 %	17
50%MEA-Kenaf	34.36	30	99.99 %	17
50%TEPA-Kenaf	40.22	30	99.99 %	17
MCM-41	35.00	25	n.a	10
$Fe_2O_3/MCM-41$	38.40	25	n.a	10
NiO	14.14	25	99 %	25
$CeO_2$	48.00	25	≥ 99.5 %	30
$Fe_2O_3$	17.00	25	99 %	31
$SiO_2$	33.73	25	99 %	32
1%[bmim][CF <sub>3</sub> SO <sub>3</sub> ]/SiO <sub>2</sub>	66.71	25	99 %	32
10%NiO/[emim][HSO <sub>4</sub> ]/SiO <sub>2</sub>	48.80	25	99 %	33
10%[emim][HSO <sub>4</sub> ]/SiO <sub>2</sub>	26.70	25	99 %	33
10%ChCl:U/SG200	22.30	30	99 %	34
ChCl:U/AC	39.40	25	15 % in N <sub>2</sub>	35

# 2. EXPERIMENTAL

# 2.1 Sample Preparation

Charcoal activated carbon (Qrec), cobalt (II) sulfate heptahydrate (Hamburg), cerium (III) nitrate hexahydrate (Nacalai Tesque), and zinc sulfate heptahydrate (R&M) were used as precursors. Moisture removal was conducted by drying the AC in an oven for 2 hours at 110 °C. AC was performed double activation by using readily purchase AC to reactivate by using KMnO4. For the support treatment, AC was weighed to 5 g and was added into a solution of 0.1 M KMnO4. The mixture was shaken for 20 minutes at 200 rpm and followed by filtering and rinsing with 200 mL distilled water. The AC was dried in an oven overnight at 110 °C. The adsorbents were prepared by a conventional wet impregnation method. Generally, 0.1 M metal

salt was prepared in a 50 mL volumetric flask. AC was added to the metal salts solution and shaken for 8 hours at 200 rpm. The mixture was filtered and rinsed with 400 mL of 1 % NaHCO<sub>3</sub> solution and followed by soaking overnight in 600 mL of 1 % NaHCO<sub>3</sub> solution. Soaked samples were filtered and rinsed with distilled water and allowed to air dry for 2 hours. The samples were dried overnight in an oven at 110 °C. The resultant adsorbents were denoted as metal oxide/activated carbon (MO/AC) where MO represents Co<sub>3</sub>O<sub>4</sub>, CeO<sub>2</sub>, ZnO.

#### 2.2 CO<sub>2</sub> Adsorption and Desorption

The CO<sub>2</sub> adsorption was measured by using thermogravimetric analysis-derivative thermogravimetry (TGA-DTG) from a Simultaneous Thermal Analyzer (STA) 6000, Perkin Elmer. Approximately 10 mg of each sample was cleaned at 350 °C in the N<sub>2</sub> atmosphere prior to adsorption measurement. The adsorbent was heated from 30 to 350 °C at 30 °C/min and was cooled to 30 °C. The CO<sub>2</sub> adsorption was conducted at 30 °C for 20 minutes. The adsorption capacity was measured from the weight gained after the saturation exposure. Finally, the gas feed was switched to the N<sub>2</sub> atmosphere and was heated again up to 900 °C for the desorption process. The carbonate dissociation temperature was determined to perform the recyclability test at different adsorption temperature.

#### 2.3 Adsorbent Characterization

The infrared spectra of various metal oxides supported on AC were recorded between 400 and 4000 cm<sup>-1</sup> using FTIR (PerkinElmer) with KBr pellet method for sample preparation. N<sub>2</sub> adsorption-desorption isotherms were measured on a static volumetric technique instrument (Micromeritics ASAP 2020) for determination of the BET surface area, mesopore surface area, micropore surface area, total pore volume, micropore volume, and the average pore diameter. The pore size distribution was computed using DFT method. Approximately 0.5 g of each adsorbent was degassed at 350 °C under vacuum prior to the measurement for the elimination of humidity gases trapped in the adsorbents. A water circulating bath was used to control the temperature. The N<sub>2</sub> adsorption-desorption isotherms were recorded at liquid nitrogen temperature of 77 K, and applied in a relative pressure (P/Po) ranging from 0 to 1.0. The surface area (S<sub>BET</sub>) was calculated by using a commonly used method called Brunauer-Emmett-Teller (BET) method. All surface area measurements were calculated from the nitrogen adsorption-desorption isotherms by assuming the N<sub>2</sub> molecule to be 0.162 nm<sup>2</sup>. The t-plot method was used to calculate the mesopore surface area (S<sub>meso</sub>), micropore surface area (S<sub>micro</sub>) and micropore

volume ( $V_{micro}$ ). The total pore volume ( $V_{tot}$ ) was obtained by converting the amount of  $N_2$  gas adsorbed (in cm<sup>3</sup>/g at STP) at relative pressure to the volume of gas adsorbate.

The most efficient adsorbent was characterized by its phase composition and surface morphology. X-ray Diffraction (XRD) pattern was obtained by using XRD diffractometer (Bruker D8 Advance). The crystal structures were verified by recording 2θ diffraction angle from 10° to 70° and matched with standard diffraction data (JCPDS) file for interpretation of the crystalline phase. The surface micrograph of the most efficient adsorbent was observed using a scanning electron microscope (Quanta 650 field emission gun SEM).

# 2.4 Adsorption optimization and recyclability test

The most efficient adsorbent was optimized with different adsorption temperatures of 30 and 50 °C. The recyclability test was performed for 5 cycles of CO<sub>2</sub> adsorption and desorption by using the aforementioned TGA-DTG analysis. Generally, for the first cycle, the adsorbent will start with the cleaning process, cooled to desirable adsorption temperature (30 or 50 °C), CO<sub>2</sub> adsorption, and CO<sub>2</sub> desorption process. After cooling to desirable adsorption temperature, the second cycle CO<sub>2</sub> adsorption starts again and followed by the desorption process. These methods were repeated up to 5 times to determine the regeneration properties of selected adsorbents.

# 2.5 Adsorption kinetics study

The experimental data for CO<sub>2</sub> adsorption of the most efficient adsorbent at different adsorption temperatures were analyzed with kinetic models such as the pseudo-first-order kinetic model and pseudo-second-order kinetic model. The adsorption kinetics describes CO<sub>2</sub> uptake rate controls with adsorption time of adsorbate uptake at the solid and gas interface.

#### 3. RESULTS AND DISCUSSION

#### 3.1 Adsorbent characterization

FTIR spectra were recorded to investigate the functional groups of activated carbon before and after impregnation with various metal oxides as it offers the properties of molecules and characteristics of chemical bonds. The IR spectra and absorption bands are shown in Figure 1 and Table 2 respectively. A typical band at 3406 cm<sup>-1</sup> is indicative of O-H stretching due to the hydrogen bond caused by moisture content in the sample<sup>22</sup>. The intensity of the strong band

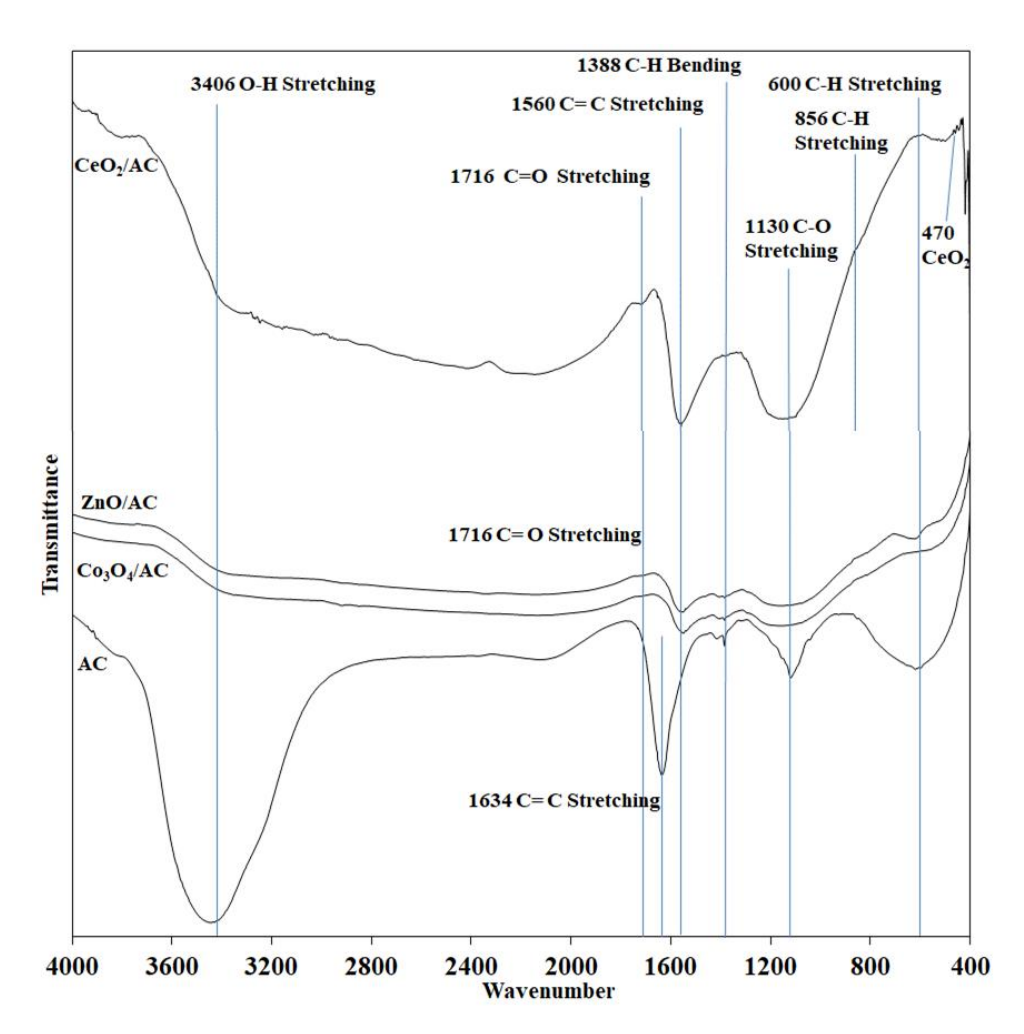


**Figure 1.** IR spectra of AC and various MO/AC.

**Table 2.** Vibrational frequencies IR spectroscopy of various MO/AC.

Vibrational modes	This study (cm <sup>-1</sup> )	Reference (cm <sup>-1</sup> )
O-H Stretching	3406	3412
C=O stretching	1716	1716
C=C Stretching	1634	1633
C=C Stretching	1560	1550
C-H Bending	1388	1390
C-O Stretching	1130	1130
C-H Stretching	600	600
Ce-O	470	459

The bands at 1643, 1388 and 600 cm<sup>-1</sup> are reported to be characteristic absorption bands of activated carbon corresponding to C=C stretching, C-H bending and C-H stretching respectively<sup>36</sup>. The decrease of intensities in these bands after impregnation with metal oxides is indicative of the deposition of metal oxides has reduced the absorption bands for AC<sup>37</sup>. Nonetheless, reactivating the AC for the MO/AC adsorbents contribute to the alteration of surface nature by introducing oxygen-containing functional groups of C=O at 1716 cm<sup>-1</sup> and changing intensities for C-O stretching at 1130 cm<sup>-1</sup>. This explains KMnO<sub>4</sub> oxidizing the surface of AC, besides forming pores structure which is in agreement with Zhang *et al.*<sup>38</sup>. The peak at 1634 shows a large redshift of 74 cm<sup>-1</sup> compared to 1560 cm<sup>-1</sup>, after loading of metal oxides which also occurred in a study conducted by Zhao *et al.*<sup>39</sup> using silver loaded on activated carbon. While the bands at 470 cm<sup>-1</sup> are ascribed to the characteristic bands of metal oxides CeO<sub>2</sub><sup>40</sup> respectively.

The N<sub>2</sub> adsorption-desorption isotherms are shown in Figure 2. According to IUPAC classification, all of the isotherms exhibit Type I isotherm<sup>41</sup>. The initial steep region is attributed to strong adsorption by a typical microporous material. Hysteresis loop closing at around relative pressure 0.4 can be observed in all isotherms, indicating that the mesoporosity of slit-shaped pores to be present in the samples<sup>26</sup>. The adsorbents show H4 hysteresis that associated with porous materials which indicating a narrow slit-shaped pore<sup>42</sup>. The N<sub>2</sub> adsorption-desorption isotherm for AC has the highest steep initial region ascribed from high micropore structure that easily occupied. The hysteresis of metal oxides loaded AC shows a larger area indicating of high mesopore structure. These are correlated with the textural properties tabulated in Table 3. The formation of mesopores may be due to that metal oxide burning off carbon wall and enlarging pore sizes during thermal treatment.

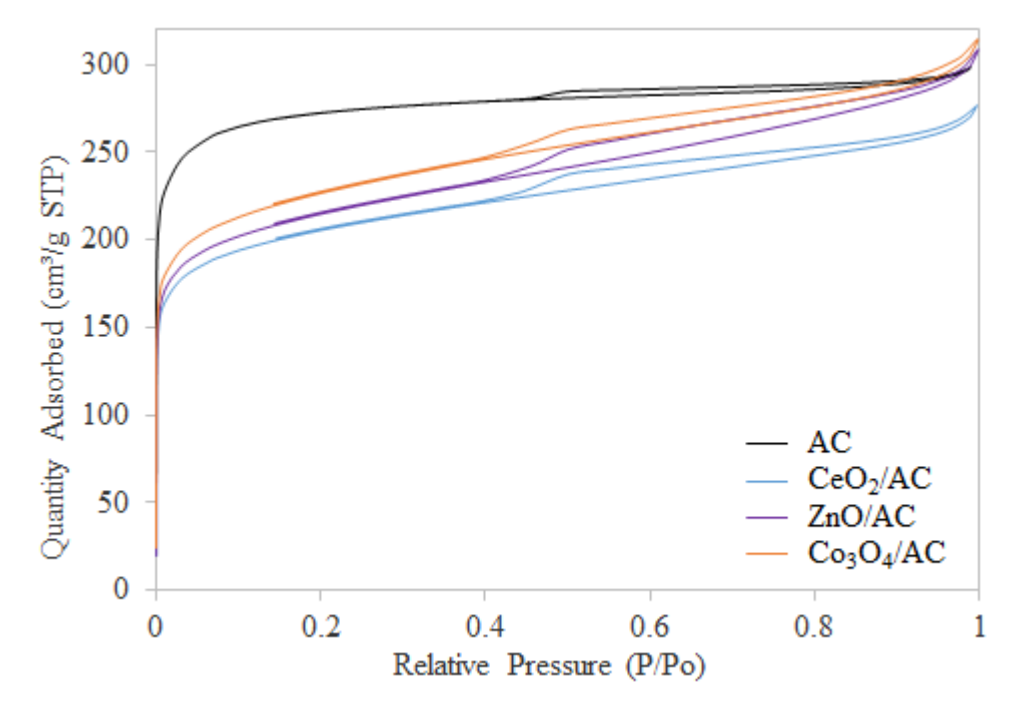


**Figure 2.**  $N_2$  adsorption-desorption isotherms of the adsorbents.

**Table 3.** The textural characteristics of the adsorbents.

Adsor	rbent	AC	CeO <sub>2</sub> /AC	ZnO/AC	Co <sub>3</sub> O <sub>4</sub> /AC
	SBET	1043.6	763.4	792.9	838.5
	$(m^2/g)$				
Surface	$S_{\text{meso}}$	171.0	254.1	280.4	302.2
area	$(m^2/g)$				
	$S_{ ext{micro}}$	872.6	509.4	512.5	536.3
	$(m^2/g)$				
	$V_{\text{total}}$	0.46	0.42	0.45	0.47
Pore	$(cm^3/g)$				
Volume	$V_{\text{micro}}$	0.35	0.21	0.21	0.22
	$(cm^3/g)$				
Averag	ge pore	1.8	2.2	2.3	2.2
diam	neter				
(nı	n)				

where  $S_{BET}$  is surface area by BET method;  $S_{mic}$  is micropore surface area by t-plot method;  $V_{total}$  is single point total pore volume;  $V_{micro}$  is micropore volume by the t-plot method

The BET surface area decreased with the loading of metal oxides onto AC samples (Table 3) indicating that the pores of the AC are blocked or covered<sup>26</sup>. However, an increase in micropore surface area and mesopore surface area ascribed from reactivation of ACs by chemical treatment with KMnO<sub>4</sub> prior to metal oxide impregnation. It is notably Co<sub>3</sub>O<sub>4</sub>/AC has a higher surface area compared to CeO<sub>2</sub>/AC and ZnO/AC. This presumes that the Co<sub>3</sub>O<sub>4</sub> particles are deposited on AC surfaces instead of pores due to larger particle size. Thus, the pores generated from Co<sub>3</sub>O<sub>4</sub> also contribute to the increment of the adsorbent's surface area. The reduction in micropore volume after impregnated with metal oxides is mainly attributed to the addition of metal oxides particles which tend to deposit on the AC surfaces, deposited on the pores and fill the pores.

The density functional theory (DFT) method was used to compute pore size distribution (Figure 3) of the microporous AC containing various metal oxides. Although AC has a lower intensity of distribution at the region of 0.9-1.2 nm as shown in the inset of Figure 3, the AC possessed the highest distribution in the region of 1.6-2.0 nm. Thus, it has a high micropore structure in which the diameter of the pores is below 2 nm. Most of the metal oxides generated unable to enter the pores below 1.2 nm because the distribution in the region is less affected. Nonetheless, the distribution in the region of 1.6-2.0 nm was diminished might be due to the possibility of the metal oxides able to enter the pores or deposited on the pores. Above the 2.1 nm, higher distribution of pore size attributed by the pores of metal oxides generated on AC.

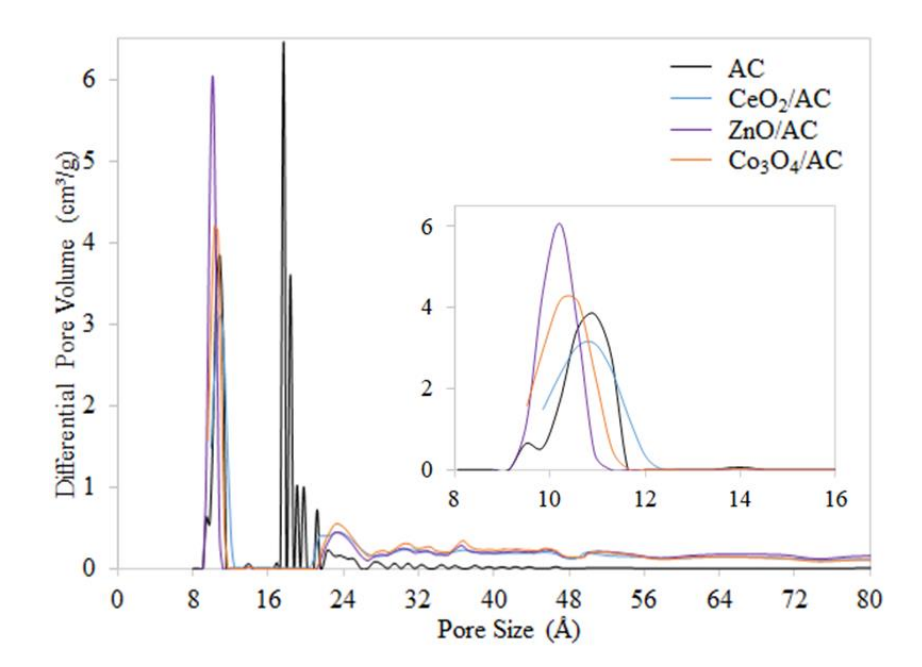


**Figure 3.** Pore size distribution.

Thermal stability of various metal oxides impregnated on AC was computed using thermogravimetric analysis by heating up to 900°C (Figure 4). The initial steep region of weight loss was attributed to moisture removal. No distinct peak of derivative weight loss was observed at higher temperature implying that the samples were resistant toward heat. The Co<sub>3</sub>O<sub>4</sub>/AC shows a derivative weight loss peak at a temperature of 830 °C which corresponded to the decomposing temperature of Co<sub>3</sub>O<sub>4</sub><sup>43</sup>. This phenomenon can be attributed to two possible factors of decomposition during thermal treatment for Co<sub>3</sub>O<sub>4</sub> is incomplete or the regeneration of Co<sub>3</sub>O<sub>4</sub>.

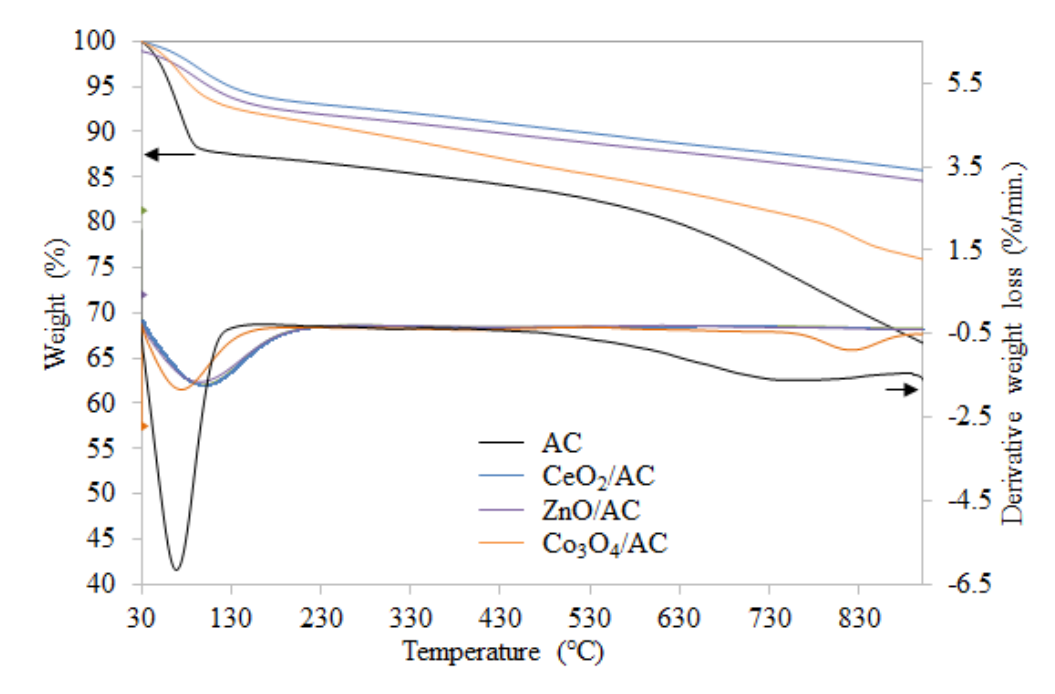


**Figure 4.** Thermal stability of the adsorbents.

### 3.2 CO<sub>2</sub> capture

CO<sub>2</sub> capture was performed using TGA and the wide-angle of the thermograms was plotted as shown in Figure 5. The CO<sub>2</sub> adsorption and desorption process are shown in the narrow-angle of Figures 6a and 6b respectively. The adsorption capacity was obtained from the weight gain of Figure 6a. At the beginning of the adsorption, it is observed that the initial steep region indicates the amount of CO<sub>2</sub> adsorbed on CeO<sub>2</sub>/AC and AC are faster than ZnO/AC and Co<sub>3</sub>O<sub>4</sub>/AC. Eventually, the adsorption gradually decreases when the progress of the adsorption process reaches equilibrium. Figure 6a demonstrated the adsorption process has reached equilibrium state at the time of 5 minutes for AC and Co<sub>3</sub>O<sub>4</sub>/AC; 10 minutes for CeO<sub>2</sub>/AC; 13 minutes for ZnO/AC. Steep initial region corresponded to stronger binding force in between

CO<sub>2</sub> with metal oxides and CO<sub>2</sub> with micropores of AC. At the knee-shaped region, the multilayer CO<sub>2</sub> adsorption on the adsorbent formed by occupying CO<sub>2</sub> adsorbate on the uneven bonded CO<sub>2</sub> surface and creating CO<sub>2</sub>-CO<sub>2</sub> interaction. It is noteworthy to observe that CeO<sub>2</sub>/AC and ZnO/AC show higher adsorption capacity at equilibrium state compared to AC only. This is indicative of CeO<sub>2</sub> and ZnO possesses higher basic properties compared to Co<sub>3</sub>O<sub>4</sub>. Whereas AC was unable to hold CO<sub>2</sub> strongly compared to those with the presence of metal oxides on AC. Although AC only exhibits the highest surface area, the adsorption capacity was observed lower than CeO<sub>2</sub>/AC. This explains reactivate the AC by using chemical activation of KMnO<sub>4</sub> may improve AC surface nature, may altering the properties of AC, including pore structure and purity. The significance of double activation increasing the oxygen functional group that resulting enhancement of AC surfaces and adsorption capacity.

Furthermore, the AC surface modification by impregnation of CeO<sub>2</sub> provides basic active sites that chiefly responsible for the formation of carbonate species and enhancing adsorption capacity. The formation of carbonate species by CO<sub>2</sub> chemisorption reaction pathway can be simplified as in Equation 2.

$$CO_2$$
 (adsorbate) + O (surface of  $CeO_2$ )  $\rightarrow$  [ $CO_2$ -O]  $\rightarrow$   $CO_3$  (chemisorption) (2)

The chemisorption allows the active sites from the oxygen surface of CeO<sub>2</sub> to exchange electron with CO<sub>2</sub> forming carbonate species product. This could be the reason for the presence of metal oxides that may hold the CO<sub>2</sub> firmly at equilibrium state compared to AC only. Lower in adsorption capacity for Co<sub>3</sub>O<sub>4</sub>/AC compared to AC only might also be attributed to the weakly adsorbed CO species by cobalt ion which can be fully desorbed at 230K (-43 °C) as reported by Ferstl *et al.*<sup>44</sup>.

The thermograms for the desorption process (Figure 6b) shows CeO<sub>2</sub>/AC has the highest weight loss up to around 400 °C for CO<sub>2</sub> regeneration. It has a relatively lower CO<sub>2</sub> desorption temperature of 160-280 °C<sup>45</sup>. Hence, the carbonate product will be dissociated to regenerate as CO<sub>2</sub> and leaving the adsorbent that suitable to be reused for the next cycle. The desorption temperature above 400 °C resulting in greater weight loss for all adsorbents. Thus, the desorption temperature up to 400 °C will be deployed for the recyclability test.

The adsorption capacity for all adsorbents and similar works were tabulated in Table 4. Among the synthesized adsorbents, CeO<sub>2</sub>/AC shows the highest adsorption capacity of 52.78 mg/g at equilibrium. Therefore, CeO<sub>2</sub>/AC was chosen as the most efficient adsorbent for further performance optimization through the recyclability test at different adsorption temperature. In comparison with unmodified AC was used to load with 10 % CeO<sub>2</sub> (ACCe-HT) and CuO (ACCu-HT) separately by using hydrothermal treatment <sup>46</sup> shows lower adsorption capacity than this work (Table 4). Meanwhile, Heo *et al.*<sup>28</sup> deployed a slightly complicated method than that of this work but obtaining a comparable CO<sub>2</sub> adsorption capacity through 12 minutes microwave radiated synthesis of MgO on microporous carbon (MC).

Several common activating agents were reported such as zinc chloride (ZnCl<sub>2</sub>), potassium hydroxide (KOH), hydrochloric acid (HCl), nitric acid (HNO<sub>3</sub>) and phosphoric acid (H<sub>3</sub>PO<sub>4</sub>)<sup>47</sup>. This study reported double activation of AC by reactivating with KMnO<sub>4</sub>. The significance of chemical activation over physical activation was reported in which chemical activation by using ZnCl<sub>2</sub> is a promising method to obtain better textural properties for AC derived from palm kernel shell (PCAC)<sup>48</sup>. By loading BaO on PCAC, it was observed to be the best adsorbent for CO<sub>2</sub> capture ascribed from the highest BET surface area. Meanwhile, Plaza *et al.*<sup>49</sup> reported AC from the spent coffee ground shows higher CO<sub>2</sub> adsorption capacity by chemical activation using KOH than physical activation.

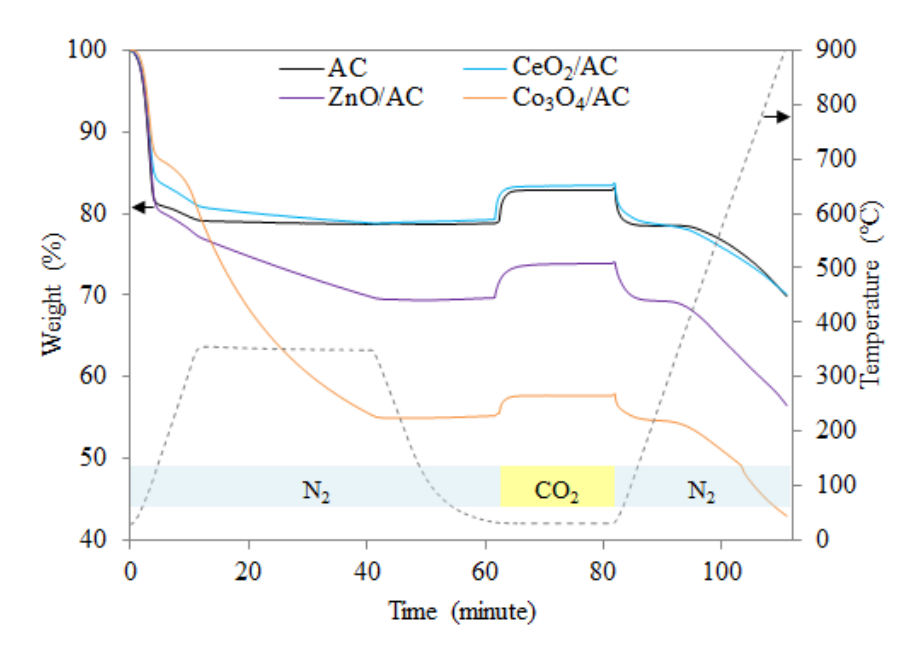


**Figure 5.** Simultaneous CO<sub>2</sub> adsorption and desorption for all adsorbents with adsorption temperature of 30 °C.

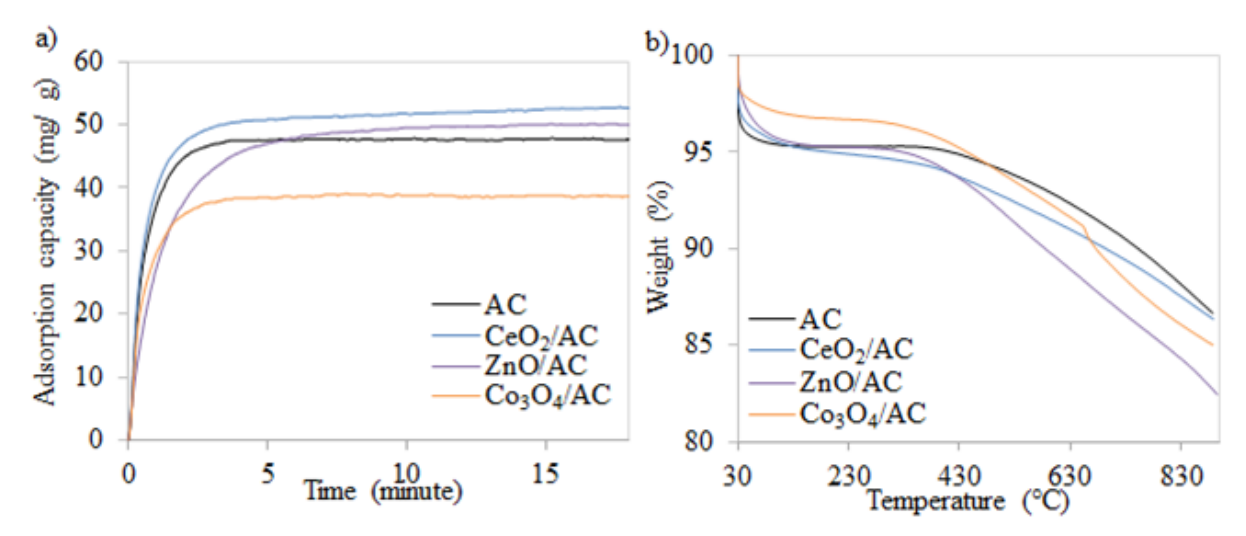


**Figure 6.** Narrow-angle for the a) CO<sub>2</sub> adsorption at 30 °C and b) desorption process.

**Table 4.** Adsorption capacities of various sorbents.

Adsorbent	Adsorption	Adsorption	$CO_2$	Sources
	Capacity (mg/g)	Temperature (°C)	Purity	
AC	52.01	30	99 %	This study
CeO <sub>2</sub> /AC	52.78	30	99 %	This study
ZnO/AC	52.06	30	99 %	This study
Co <sub>3</sub> O <sub>4</sub> /AC	43.17	30	99 %	This study
ACCe-HT	37.66	30	20 %	47
ACCu-HT	25.74	30	20 %	47
Mg-MCs-12	53.68	40	15 % in N <sub>2</sub>	28

The phase composition of CeO<sub>2</sub>/AC was determined by XRD diffractograms as shown in Figure 7. Typical graphitic structure for AC with broad amorphous diffraction peaks at 2θ values of 26° and 43°. After loading with CeO<sub>2</sub>, the amorphous peaks decreased and shifted from 26° and 43° toward 29° and 48° respectively. Another new diffraction peak was observed at 56°. These three diffraction peaks are the reflections of the (111), (220) and (311) crystallographic planes of the cubic CeO<sub>2</sub> phase<sup>50</sup>. The CeO<sub>2</sub>/AC surface morphology (Figure 8) shows the well-distributed of fine particles CeO<sub>2</sub> on AC surfaces. Reactivating the AC resulting scavenging effect to the AC surface and resulting slightly enlargement of the pore structure. The SEM image supporting the prediction from the textural properties with a possibility of the CeO<sub>2</sub> able to enter the pores of AC and deposited on AC surfaces.

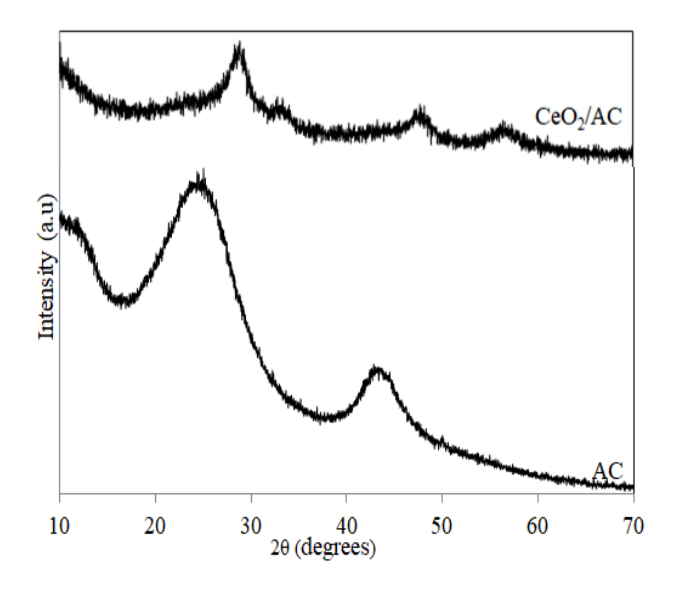


**Figure 7.** XRD diffractograms.

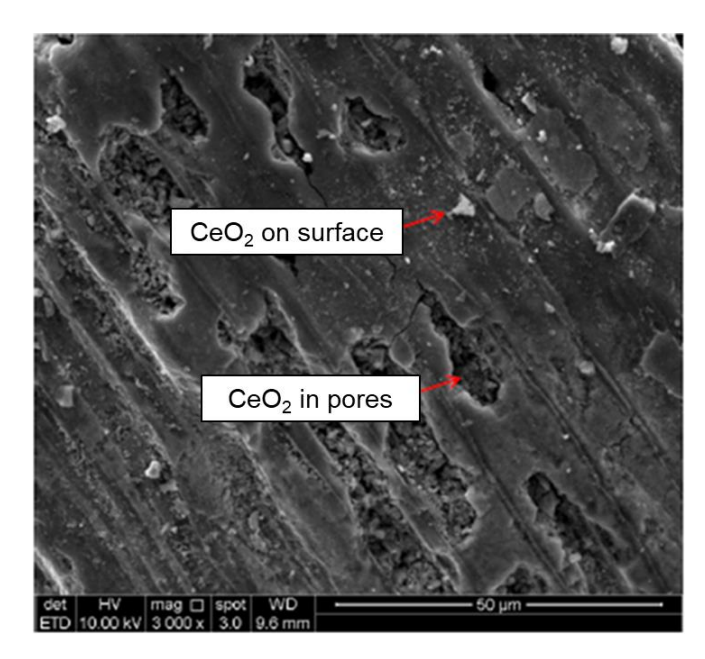


**Figure 8.** SEM images of CeO<sub>2</sub>/AC.

# 3.3 Recyclability test

Five cycles of  $CO_2$  adsorption-desorption was conducted to optimize the performance for  $CeO_2/AC$  at different adsorption temperature of 30 and 50 °C (Figure 9). It is interesting to note that the adsorption capacity is higher for the adsorption temperature of 30 °C than 50 °C. At adsorption temperature of 30 °C, the loss in adsorption capacity was only 6.53 % with a decrease from first to fifth cycles is 52.50 mg  $CO_2$ / g adsorbent to 49.07 mg  $CO_2$ / g adsorbent respectively. Whereas at adsorption temperature of 50 °C, there was a 7.86% loss in adsorption capacity with a decrease from first to fifth cycles is 40.56 mg  $CO_2$ / g adsorbent to 37.37 mg  $CO_2$ / g adsorbent respectively. This build relationship that adsorption capacity decrease as the

adsorption temperature increase. According to Rashidi *et al.*<sup>51</sup>, an exothermic process where physisorption is favored at lower temperature implies the existence of physisorption throughout the process of adsorption. Thus, at a temperature above 30 °C, the adsorbate of CO<sub>2</sub> has the tendency to desorb during the adsorption period has reach equilibrium and leads to lower adsorption capacity.

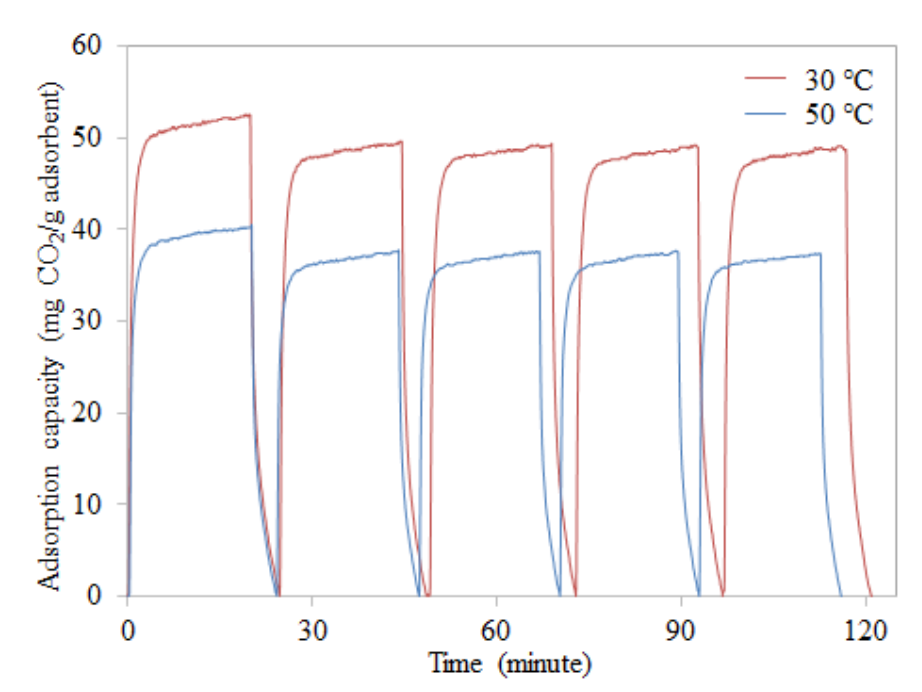


**Figure 9.** Five cycles of CO<sub>2</sub> capture at adsorption temperature of 30 and 50 °C.

#### 3.4 Kinetic Analysis

The CO<sub>2</sub> adsorption kinetics data for CeO<sub>2</sub>/AC at different operating adsorption temperatures from the first cycle was fitted by using two kinetic models namely pseudo-first-order (Equation 3), pseudo-second-order kinetic model (Equation 4).

409 
$$\log(q_e - q_t) = \log q_e - \left(\frac{k_1}{2.303}\right)t$$
 (3)

410 
$$\frac{t}{q_t} = \frac{1}{k_2 q_e^2} + \left(\frac{1}{q_e}\right) t$$
 (4)

where  $q_t$  and  $q_e$  are the adsorption capacity at any particular time t and at equilibrium respectively, and  $k_l$  is the pseudo-first-order kinetic constant,  $k_l$  is the pseudo-second-order kinetic constant and  $(k_l \cdot q_e^2)$  is initial adsorption rate. The kinetic linear plot using two equations above to evaluate the mechanism of the adsorption process is shown in Figure 10. The kinetic parameters were tabulated in Table 5.

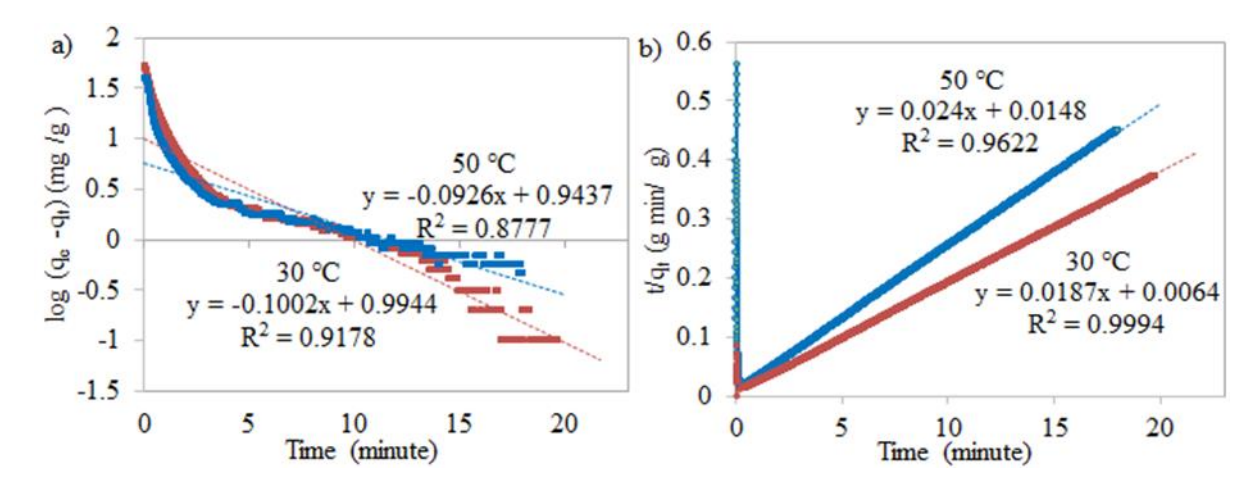


**Figure 10.** Kinetic plot a) pseudo-first-order kinetic model and b) pseudo-second-order kinetic model at different adsorption temperatures for CeO<sub>2</sub>/AC.

**Table 5.** Kinetic parameters of CO<sub>2</sub> adsorption onto CeO<sub>2</sub>/AC.

	Parameter	Temperature (°C)	
Kinetic model	Parameter	30	50
	$q_{e(act)} \ (mg/g)$	52.78	40.56
Pseudo-first order kinetic	$q_{e(cal)}$ $(mg/g)$	9.87	8.78
	$k_1(1/min)$	0.2308	0.2132
	$\mathbb{R}^2$	0.9178	0.8777
	Relative error (%)	81.29	78.34
Pseudo-first order kinetic	$q_{e(cal)}$ $(mg/g)$	53.47	41.67
	k <sub>2</sub> (g/mg	00546	0.0389
	min)		
	h (mg/g min)	156.14	67.57
	$\mathbb{R}^2$	0.9994	0.9622
	Relative error (%)	1.32	2.74

where  $q_{e(act)}$  = actual adsorption capacity;  $q_{e(cal)}$  = calculated adsorption capacity

Pseudo-second-order kinetic model shows the correlation coefficient values of  $R^2$  are 0.9994 and 0.9622 for both adsorption temperatures of 30 and 50 °C respectively. The relative error between actual adsorption capacity and calculated adsorption capacity shows only 1.32 and 2.74 % for adsorption temperatures of 30 and 50 °C respectively. The pseudo-first-order kinetic model shows high  $R^2$  at 0.9178 and 0.8777 for  $CO_2$  adsorption at 30 and 50 °C respectively. Nonetheless, the calculated adsorption capacity significantly deviates from the actual adsorption capacity with a relative error of 81.29 and 78.34 % for adsorption temperatures at

30 and 50 °C respectively. Based on these R<sup>2</sup> values and relative errors, the pseudo-second-order kinetic model fits the CO<sub>2</sub> adsorption kinetic profiles relatively better than the pseudo-first-order kinetic model at both adsorption temperatures of 30 and 50 °C. This suggests the CO<sub>2</sub> adsorption incline towards chemisorption although both of the physisorption and chemisorption have existed. It might be the limiting step involving the exchange electron between CeO<sub>2</sub> and CO<sub>2</sub> adsorbate resulting in the adsorption process mainly governed by monolayer adsorption referring to chemical phenomena. This proving that AC surface reactivation with the addition of CeO<sub>2</sub> could enhance the adsorption capacity by chemisorption.

#### 4. **CONCLUSION**

Various metal oxides impregnated on chemically reactivate of AC were successfully synthesized. SEM images and XRD pattern confirm that CeO<sub>2</sub> were highly dispersed on the AC surface. FTIR showed the characteristic peaks for the increased oxygen-containing functional group on activated carbon. All the MO/AC showed great thermal stability with high resistance toward heat up to 900 °C except Co<sub>3</sub>O<sub>4</sub>/AC. The CeO<sub>2</sub>/AC exhibited the most efficient adsorbent with an adsorption capacity of 52.78 mg/g at the equilibrium state of 10 minutes. It showed only a 6.53% loss in adsorption capacity after five cycles and a relatively lower desorption temperature of 160-280 °C which requires less energy consumption. The pseudo-second-order kinetic model was best fitted compared to the pseudo-first-order kinetic model with a relatively higher correlation coefficient which implies not only physisorption but chemisorption is significant for CeO<sub>2</sub>/AC.

#### 5. ACKNOWLEDGEMENT

The authors are grateful to the Department of Science and Technology, Universiti Putra Malaysia Kampus Bintulu and School of Chemical Sciences, Universiti Sains Malaysia for the research facilities. The authors wish to thanks the Ministry of Higher Education for the financial support for grant numbers of GP-IPM-9657200, GP-IPM-9559000, 1001.PKIMIA.811333 and 1001.PKIMIA.822215.

#### 6. REFERENCES

- 1. National Oceanic and Atmospheric Administration (NOAA), Recent Global CO<sub>2</sub>, https://www.esrl.noaa.gov/gmd/ccgg/trends/global.html (accessed: March 3<sup>rd</sup>, 2020)
- 463 2. N. Mimura, P. Jpn. Acad. B Phys. Bio. Sci. 2013, 89(6), 281-301.

- 464 3. J. R. Fanchi, C. J. Fanchi, Energy in the 21st Century, Fourth Edition, World Scientific,
- Singapore, Singapore, **2016**.
- 466 4. B. Metz, O. Davidson, H. D. Coninck, M. Loos, L. Meyer, IPCC special report on
- carbon dioxide capture and storage, Cambridge University Press, New York, United
- 468 States, **2005**.
- 469 5. W. Yuan, Z. Li, A. Otto, M. Robinius, D. Stolten, *Energy Procedia*. **2017**, 114, 650-
- 470 665.
- 471 6. E. S. Kikkinides, R. T. Yang, S. H. Cho, *Ind. Eng. Chem. Res.* **1993**, *32*, 2714-2720.
- 472 7. Q. Wang, Q. J. Luo, Z. Zhong, A. Borgna, *Energ. Environ. Sci.* **2011**, *4*(1), 42-55.
- 473 8. J. Gale, Y. Kaya, Greenhouse Gas Control Technologies, Pergamon, New York, United
- 474 States, **2003**.
- 475 9. C. H. Yu, C. H. Huang, C. S. Tan, Aerosol Air Qual. Res. 2012, 12(5), 745-769.
- 476 10. K. C. Chanapattharapol, S. Krachuamram, S. Youngme, *Micropor. Mesopor. Mat.*
- **2017**, *245*, 8-15.
- 478 11. A. E. Ogungbenro, D. V. Quang, K. Al-Ali, M. R. M. Abu-Zahra, Energy Procedia.
- **2017**, *114*, 2313-2321.
- 480 12. R. Kodasma, J. Fermoso, A. Sanna, *Chem. Eng. J.* **2018**, *358*, 1351-1362.
- 481 13. C. E. Bien, K. K. Chen, S. C. Chien, B. R. Reiner, L. C. Lin, C. R. Wade, W. S. W. Ho,
- 482 *J. Am. Chem. Soc.* **2018**, *140*(40), 12662-12666.
- 483 14. S. S. Shang, A. Hanif, M. Z Sun, Y. M. Tian, Y. S. Ok, I. K. M.Yud, D. C.W. Tsang,
- 484 Q. F. Gue, J. Shang, J. Hazard, Mater. 2019, 373, 285-293.
- 485 15. M. N. Abu Tahari, A. Hakim, T. S. Marliza, N. H. Mohd, M. A. Yarmo, *Mater. Sci.*
- 486 Forum **2017**, 888, 529-533.
- 487 16. M. A. Naeem, A. Armutlulu, Q. Imtiaz, C. R. Meller, ChemPhysChem. 2017, 18, 3280-
- 488 3285.
- 489 17. A. Boonpoke, S. Chiarakorn, N. Laosiripojana, S. Towprayoon, Korean J. Chem. Eng.
- **2012**, *29*, 89-94.
- 491 18. K. S. N. Kamarudin, N. Zaini, N. E. A. Khairuddin, *J. Environ. Chem. Eng.* **2018**, 6,
- 492 549-559.
- 493 19. S. Lin, T. Kiga, Y. Wang, K. Nakayama, *Energy Procedia* **2011**, *4*, 356-361.
- 494 20. S. C. Tian, J. G. Jiang, F. Yan, K. M. Li, X. J. Chen, V. Manovic, *Green Chem.* 2016,
- 495 *18*, 4022-4031.

- 496 21. S. Wongsakulphasatch, K. Sukchoknamchai, N. Suthapot, W. Praikaew, C. Chaisuk, W.
- 497 Kiatkittipong, N. Laosiripojana, S. Assabumrungrat, S. MATEC Web of Conferences
- **2018**, 192, 03057.
- 499 22. A. Hakim, T. S. Marliza, M. N. Abu Tahari, W. N. R. Wan Isahak, M. R. Yusop, M. W.
- 500 Mohamed Hisham, M. A. Yarmo, *Ind. Eng. Chem. Res.* **2016**, *55*(29), 7888-7897.
- 501 23. J. Baltrusaitis, J. Schuttlefield, E. Zeitler, V. H. Grassian, 2011. Chem. Eng. J. 2011,
- 502 *170*, 471-481.
- 503 24. K. Yoshikawa, H. Sato, M. Kaneeda, J. N. Kondo, J. CO<sub>2</sub> Util. 2014, 8, 34-38.
- 504 25. Y. M. Wang, R. Kováčik, B. Meyer, K. Kotsis, D. Stodt, V. Staemmler, H. S. Qiu, F.
- Traeger, D. Langenberg, M. Muhler, C. Wöll, Angew. Chem. Int. Edit. 2007, 46, 5624-
- 506 5627.
- 507 26. A. Hakim, M. N. Abu Tahari, T. S. Marliza, W. N. R. Wan Isahak, M. R. Yusop, M. W.
- 508 M. Hisham, M. A. Yarmo, J. Teknol. (Sci. Eng.). 2015, 77(33), 75-84.
- 509 27. A. Hakim, W. N. R. Wan Isahak, M. N. Abu Tahari, M. R. Yusop, M. H. Mohamed
- 510 Wahab, M. A. Yarmo, *Adv. Mat. Res.* **2015**, *1087*, 45-49.
- 511 28. Y. J. Heo, S. J. Park, Sci. Rep. 2017, 5653, 1-9.
- 512 29. W. N. R. Wan Isahak, Z. A. Che Ramli, A. Z. Lahuri, M. R. Yusop, M. H. Mohamed
- 513 Wahab, M. A. Yarmo, *Adv. Mat. Res.* **2015**, *1087*, 111-115.
- 514 30. C. Slotowski, S. Marre, P. Dagault, O, Babot, T. Toupance, C. Aymonier, J. CO<sub>2</sub> Uti.,
- **2017**, *20*, 52-58.
- 516 31. A. Hakim, M. A. Yarmo, T. S. Marliza, M. N. A. Tahari, W. Z. Samad, M. R. Yusop, M.
- 517 W. M. Hisham, N. Dzakaria, *Malaysian J. Anal. Sci.* **2016**, 20(6), 1286-1298.
- 518 32. T. S. Marliza, M. A. Yarmo, A. Hakim, M. N. A. Tahari, Y. H. Taufiq-Yap, *Mater. Sci.*
- 519 Forum, **2017**, 888, 485-490.
- 520 33. T. S. Marliza, M. A. Yarmo, A. Hakim, M. N. A. Tahari, M. W. M. Hisham, Y. H.
- 521 Taufiq-Yap, AIP. **2017**, 20008, 1-8.
- 522 34. Z. Ghazali, N. H. Hassan, M. A. Yarmo, L. P. Teh, R. Othaman, Sains Malays. 2019,
- *48*(*5*), 1025-1033.
- 524 35. N. Z. Zulkurnai, U. F. Md. Ali, N. Ibrahim, N. S. Abdul Manan, E3S Web Conf. 2018,
- *34*, 02030.
- 526 36. S. Ge, Z. Liu, Y. Furuta, W. Peng, Saudi J. Biol. Sci. 2017, 24(6), 1370-1374.
- 527 37. G. Zhang, J. Qu, H. Liu, A. T. Cooper, R. Wu, Chemosphere **2007**, 68(6), 1058-1066.
- 528 38. G. Zhang, Y. Sun, P. Zhao, Y. Xu, A. Su, J. Qu, J. CO<sub>2</sub> Util. **2017**, 20, 129-140.
- 529 39. H. Zhao, F. Wang, Y. Ning, B. Zhao, F. Yin, Y. Lai, K. Hu, Sci. Rep. 2013, 3, 1511.

- 530 40. G. H. Hara Priya, N. Sunganya, V. Jaisankar, Int. J. Adv. Chem. Sci. Appl. 2015, 3, 6-
- 531 14.
- 532 41. K. S. W. Sing, D. H. Everett, R. A. W. Haul, L. Moscou, R. A. Pierotti, J. Rouquerol,
- 533 Pure & Appl. Chem. **1985**, 57(4), 603-619.
- 534 42. J. B. Condon, Surface Area and Porosity Determinations by Physisorption:
- Measurements and Theory, first ed., Oxford, United Kingdom, Elsevier B. V., **2006**.
- 536 43. G. A. El-Shobaky, A. S. Ahmad, A. N. Al-Noaimi, H. G. El-Shobaky, J. Therm. Anal.
- **1996**, *46*(6), 1801-1808.
- 538 44. P. Ferstl, S. Mehl, M. A. Arman, M. Schuler, A. Toghan, B. Laszlo, J. Knudsen, J. Phys.
- 539 *Chem. C* **2015**, *119*(29), 16688-16699.
- 540 45. V. Savin, V. Sobolev, Z. Eremenko, Z. Grigor'eva, J. Anal. Chem.-USSR. 1985, 59(3),
- 541 571-575.
- 542 46. H. Madzaki, W. A. W. A. K. Ghani, S. Y. Thomas Choong, U. Rashid, N. Muda, J.
- 543 *Kejuruteraan.* **2018**, *30*(1), 31-38.
- 544 47. I. Senturk, M. Alzein, Acta Chim. Slov. 2020. 67, 1-15.
- 545 48. A. R. Hidayu, N. Muda, *Procedia Eng.* **2016**. 148, 106-113.
- 546 49. M. G. Plaza, A. S. Gonzalez, C. Pevida, J. J. Pis, F. Rubiera, Appl. Energy. 2012, 99,
- 547 272-279.
- 548 50. H. Qin, H. Chen, X. Zhang, G. Yang, Y. Feng, J. Chem. Technol. Biot. 2014, 89(9),
- 549 1402-1409.

550 51. N. A. Rashidi, S. Yusup, B. H. Hameed, *Energy.* **2013**, *61*, 440-446.